



HAL
open science

Photo-assisted SCR over highly dispersed silver sub-nanoparticles in zeolite T under visible light: An Operando FTIR study

Houeida Issa Hamoud, Mama Lafjah, Fatima Douma, Oleg Lebedev, Fatiha Djafri, Valentin Valchev, Marco Daturi, Mohamad El-Roz

► To cite this version:

Houeida Issa Hamoud, Mama Lafjah, Fatima Douma, Oleg Lebedev, Fatiha Djafri, et al.. Photo-assisted SCR over highly dispersed silver sub-nanoparticles in zeolite T under visible light: An Operando FTIR study. *Solar Energy*, 2019, Recent Advances in Solar Photocatalysis, 189, pp.244-253. 10.1016/j.solener.2019.07.020 . hal-02400485

HAL Id: hal-02400485

<https://hal.science/hal-02400485>

Submitted on 5 Oct 2021

HAL is a multi-disciplinary open access archive for the deposit and dissemination of scientific research documents, whether they are published or not. The documents may come from teaching and research institutions in France or abroad, or from public or private research centers.

L'archive ouverte pluridisciplinaire **HAL**, est destinée au dépôt et à la diffusion de documents scientifiques de niveau recherche, publiés ou non, émanant des établissements d'enseignement et de recherche français ou étrangers, des laboratoires publics ou privés.

Photo-assisted SCR over highly dispersed silver sub-nanoparticles in zeolite under visible light: an *Operando* FTIR study

Houeida Issa Hamoud,^a Mama Lafjah,^b Fatima Douma,^{a,b} Oleg I. Lebedev,^c Fatiha Djafri,^b Valentin Valchev,^a Marco Daturi,^a Mohamad El-Roz^{a*}

^a Normandie Université, ENSICAEN, UNICAEN, CNRS, Laboratoire Catalyse et Spectrochimie, 14000 Caen, France.

^b Université d'Oran 1, Laboratoires de Chimie des Matériaux, Algeria.

^c Normandie Université, ENSICAEN, UNICAEN, CNRS, CRISMAT, 14000 Caen, France.

* Corresponding author: mohamad.elroz@ensicaen.fr

Abstract

In this study, the photo-assisted SCR-NH₃ activities of vanadium containing zeolite X (ZX-V) and Ag@ZX-V catalysts are investigated under visible-light and soft temperature conditions (RT and T = 150 °C). The highly dispersed silver was incorporated into the zeolite structure as Ag_n^{δ+} nano and sub-nano-clusters with small particle size (< 1 nm) using a new photochemical concept. The catalysts were characterized using different techniques such as XRD, N₂ sorption, H-TEM, and DR-UV-Vis. An *in situ* FTIR study of adsorbed CO was also performed for the characterization of the metal sites and their accessibility. The catalytic reaction was investigated using the *operando* FTIR technique allowing the study of both Ag@ZX-V and ZX-V catalytic surfaces, and the gas phase of the reaction in real time. Both catalysts are not active in dark and only Ag@ZX-V exhibits a photocatalytic activity under visible light. At RT, the results show that silvers clusters promote the photocatalytic oxidation of NH₃/NO, and no SCR is observed. This probably due to an energy transfer from the metallic site to the triplet oxygen and the formation of highly oxidant singlet oxygen. However, at T

=150 °C a significant photo-assisted SCR activity is observed under visible light irradiation with more than 18 % of additional NO_x removal. The different behavior of the material at 150°C in respect to its activity at RT is mainly attributed to the additional formation of silver nanoparticles and to the possible formation and conversion of intermediates that are not formed and or converted at RT (thermodynamic limitation). Basing on this study, a possible mechanism of the photo-assisted SCR reaction is proposed.

Keywords: Photo-assisted SCR, Silver clusters, Zeolite, Photocatalysis, Plasmon.

1. Introduction

Nitrogen oxides (NO_x) from diesel engines contribute substantially to air pollution (Larrubia et al., 2001). Selective Catalytic Reduction (SCR) with NH₃ is one of the most effective technologies to control automotive NO_x emissions. Most of the SCR catalysts possess a high activity at the intermediate and high temperature ranges (200-500 °C) (Gao et al., 2013). The development of active SCR catalyst at a lower temperature (< 200 °C), during the engine start-up, is very challenging due to the presence of excess H₂O and adsorption competition between ammonia and combustion residuals on active sites (Malpartida et al., 2011). In this regard, a combined strategy between LNT (Lean NO_x Trap) and SCR is necessary, which significantly increases the SCR operational costs and complexity (Castoldi et al., 2011; Xu et al., 2012).

Among the catalysts reported for the low-temperature SCR, single and mixed metal oxides catalysts containing Cr, Mn, Ce, Fe, Co, Ag, V, Ni and/or Cu oxides have been studied, combining the synergetic catalytic effect of the different components (Thirupathi et al. 2011; Park et al. 2013; Huang et al., 2015). For example, silver clusters (Ag_n^{δ+}) have previously been identified as the prime species for the activity of Ag/Al₂O₃ in H₂-assisted NH₃-SCR (Strömet

al., 2018), and it has been shown that the activity is linearly proportional to the relative amount of these clusters. However, these catalysts still present several drawbacks, such as the need of H₂ to form a proton on Al₂O₃, which directly participates in the reaction mechanism, the poor N₂ selectivity and low deNO_x performance at low temperature (<200 °C) (Ström *et al.*, 2018).

Photo-assisted selective catalytic reduction of NO_x under visible light is a promising approach for a significant decrease in the SCR reaction temperature. The active species can be generated at a relatively low temperature ensuring the oxidation-reduction reaction involved in the SCR process. Tanaka *et al.* have studied the photo-assisted selective catalytic reduction of NO with NH₃ over a series of TiO₂ based photocatalysts such as: TiO₂ modified by transition metal (i.e, V, Cr, Mn, Fe, Co, Ni, Cu, Zn, Y, Zr, Nb, Mo, Ta or W) (Yamazoe *et al.*, 2008; Yamamoto *et al.* 2015) and dye-modified TiO₂ (Yamamoto *et al.*, 2014a, 2015b). In the TiO₂ system, more than 80 % of NO conversion and approximately 100 % of selectivity can be achieved at a gas hourly space velocity (GHSV) of 8000 h⁻¹ at 160 °C. However, the TiO₂ has a low absorbance and activity in the visible range of light. The modification of the TiO₂ with dyes can enhance significantly its activity under visible light. On the other hand, these molecules have weak stability under the reaction condition required for photo-SCR reaction (the presence of oxidant species promotes the degradation of the dyes at relatively high temperature). Recently, Lia *et al.* (2018) have studied the photo-SCR of NO over rare-earth natural clay coupled with reduced graphene oxide under simulated solar-light irradiation. About 70 % of NO conversion and 100% N₂ selectivity were obtained at room temperature. Unfortunately, the complexity of such a system and their high-cost multi-step preparation method limit their practical use in diesel cars. Thus, developing new stable, and low-cost materials which can work at low-temperatures and high-GHSV SCR conditions remains a great challenge. More recently, we have successfully synthesized sub-nanometer silver clusters with enhanced narrow size distribution using the uniform size cages of FAU-type zeolite as a

scaffold (El-Roz et al., 2018). The sub-nanometer Ag clusters show an exceptional photocatalytic activity and selectivity for the reforming of formic acid to H₂ and CO₂ under visible light. The photocatalytic activity was assigned to the plasmonic behavior of the Ag_n^{δ+} clusters. The high performance of these materials in photocatalysis under visible light makes them very promising candidates for the photo-assisted SCR reaction especially at low temperatures, in the so-called cold-start domain.

In this study, sub-nanometer silver cluster in FAU-type zeolite were studied in the photo-assisted reaction at room temperature and 150 °C using *operando* FTIR spectroscopy. The first part of the paper is dedicated to the preparation and the physicochemical and textural characterization of the catalysts. Then, the performance of the prepared catalysts for the SCR-NH₃ reaction under different conditions of temperature and irradiation is reported, and a possible reaction mechanism is discussed.

1. Experimental part

1.1. Materials

Sub-nanometer silver clusters in nanosized zeolite ZX-V (FAU-type, 10-30 nm, Si/Al = 1.63) were prepared in two-steps, as described in reference (El-Roz et al., 2018). In the first step, the nanosized vanadium-containing zeolite X (ZX-V) was synthesized from a clear precursor suspension with a molar composition: 10 SiO₂: 1.1 Al₂O₃: x V₂O₅: 9 Na₂O : 122 H₂O. Sodium vanadate was selected as a precursor of the photoactive sites due to the efficiency of the vanadate sites for silver ion reduction versus water oxidation (formation of OH radicals and oxidant species are prevented). The properties of this precursor are fully compatible with the synthesis of the organic-template-free zeolite (same counter ions, low polymerization at high pH, etc.). The initial reactants were mixed to prepare two initial solutions denoted A and B. Solution A was prepared by dissolving 0.296 g aluminum powder (325 mesh, 99.5%, Alfa

Aesar) and 2.5 g NaOH (Aldrich, 97%) in 3 g double distilled H₂O. Vanadium containing samples were prepared by adding 0.122 g of VO₃Na (2 wt.%, in respect to the Silica and Alumina content) to this solution and stirring for 3 h. Solution B was prepared by mixing 10 g colloidal silica (Ludox-HS 30, Aldrich) with 1.077 g of NaOH and 1 g double distilled H₂O. The resulting turbid suspensions were placed in an oven at 100 °C for 5 minutes to obtain water clear suspensions. Solution A was added drop wise under vigorously stirring to the solution B at 4 °C using an ice-bath. The resulting colorless suspensions were stirred 24 h at room temperature followed by dehydration of 6 to 6.5 g H₂O (\approx 40 M H₂O from the general gel composition). Hydrothermal crystallization was conducted at 50 °C for 36 h. The nanoparticles of ZX-V were recovered by centrifugation (25 min, 20000 rpm) followed by re-dispersion in double distilled water. The procedure was repeated till reaching pH \sim 8. The second step was devoted to the preparation of Ag@ZX-V by dispersing ZX-V (zeolite concentration = 3 mg/ml) in water solutions containing ethanol as an electron donor (water:ethanol=3:1; with total volume = 20 mL) and silver nitrate as a silver precursor (3 mM). The reduction of silver ions is performed by UV irradiation of the solution for 5 min under stirring using a polychromatic Hg-Xe lamp (200 W). Less than 3 minutes of UV irradiation was enough to change the color of the milky suspension to green. This typical color modification is due to the formation of reduced silver particles in the solution. The essential role of vanadate and ethanol confirms the photocatalytic behavior of the process. The experiments were repeated many times until obtaining 200 mL of Ag@ZX-V solution. The solid was recovered by centrifugation (25 min, 20000 rpm) followed by re-dispersion in double distilled water and the procedure was repeated two times in order to remove the excess of free silver and silver precursor. Then, the suspension was dried at 50 °C under atmospheric condition.

1.2. Techniques

X-Ray Diffraction (XRD) analyses of the ZX-V and Ag@ZX-V materials were carried out with PANalytical X'Pert Pro diffractometer with $\text{CuK}\alpha$ irradiation ($\lambda = 1.5418 \text{ \AA}$). Rietveld refinements were then performed with the JANA2006 software (Palatinus et al. 2007) on PXRD data recorded on a Bruker D8-vario1 diffractometer equipped with a primary germanium (111) Johansson monochromator ($\lambda\text{K}\alpha 1 = 1.5406 \text{ \AA}$) and a LynxEye detector. The PXRD diagrams were recorded at room temperature between 5 and 50° (2θ) with a step size of $\sim 0.014^\circ$. Variable divergent slits with a constant illuminated sample length of 6 mm were used. Phase identifications were performed with the PANalytical High Score plus program. The crystal structure of Ag@ZX-V was solved by *ab initio* method using the SUPERFLIP software (El-Roz et al., 2018).

Nitrogen adsorption/desorption measurements were performed with an ASAP 2020 MP instrument. The specific surface area was calculated with the BET equation while the pore volumes were determined by the BJH method. Prior to the measurements, samples were outgassed *in situ* at 150°C for 3 h .

Advanced transmission electron microscopy (TEM), high-angle annular dark field scanning TEM (HAADF-STEM) together with EDX mapping experiments were carried out on an aberration probe and image corrected JEM ARM200F cold FEG microscope operated at 200 kV equipped with a CENTURIO EDX detector and GIF Quantum spectrometer.

DR-UV-Vis spectra of the dried powder samples were recorded by using a Cary 4000 UV-Vis spectrophotometer and a RSA-CU40 Diffuse Reflectance cell.

In situ FTIR spectroscopy of CO chemisorption was performed in order to determine the nature and the oxidation state of active sites and their accessibility. The samples (pellet of $\sim 20 \text{ mg}$) were first heated under vacuum ($< 10^{-6} \text{ mbar}$) at 150°C during 2 h . Doses of CO (between

1 and 40 torr) were then put in contact with each sample until saturation. The IR spectra were recorded with a Nicolet 6700 FTIR spectrometer equipped with a DTGS detector at a spectral resolution of 4 cm⁻¹ by accumulating 128 scans.

1.3. (Photo)Catalytic tests

For the *operando* experiments, a ‘sandwich like’ IR cell-reactor was used to analyze the catalysts surface and measure their SCR activity at the steady-state (El-Roz et al., 2017). First, the catalyst (shaped as a pellet of ~ 20 mg) was pretreated at room temperature under Ar and irradiation using a Xe-lamp (LC8 Hamamatsu, 200 W) with cut-UV filter ($\lambda > 390\text{nm}$). The lamp irradiance was measured using ILT950 spectrilight spectroradiometer from International Light Technologies. Then, the reaction was studied at RT and 150 °C in the dark or under irradiation. The full flow gas composition is reported in Table 1.

Table1.

The total flow rate was fixed at 31 cc.min⁻¹. The relative concentrations of the effluent gas were continuously measured by Mass Spectrometry (Quadrupole Pfeiffer Omnistar GSD 301) and stabilized before being sent to the cell. Finally, the composition of the output gas from the IR reactor cell, including NO, NO₂ and NO_x, was analyzed simultaneously by Chemiluminescence (Thermo-Scientific, model 42 i-HL) and IR spectrometer (ThermoNicolet NEXUS 670 FTIR) equipped with an MCT detector with a spectral resolution of 4 cm⁻¹ and accumulating 64 scans. The NO_x conversions were calculated from the equations (1) at the steady-state (after at least 1 hour of reaction). It should be noted that these conversions are corrected by those obtained for the same experiment performed in dark and at RT (no possible reaction is expected in this condition for both catalysts).

$$\text{NO}_x \text{ conversion } [\%] = \frac{(\text{NO}_{x,\text{inlet}} - \text{NO}_{x,\text{outlet}})}{(\text{NO}_{x,\text{inlet}})} \times 100 \quad (\text{Eq. 1})$$

2. Results and discussion

2.1. Characterizations of ZX-V and Ag@ZX-V catalysts

The X-ray diffraction patterns of the ZX-V and Ag@ZX-V samples are displayed in Figure 1(A).

Figure 1.

The ZX-V sample shows the typical Bragg pattern of FAU-type zeolite. The Rietveld refinements (Table S1 and S2 in the supplementary information) show the following chemical formula $\text{Na}_{82}\text{Al}_{73}\text{Si}_{119}\text{O}_{384}(\text{H}_2\text{O})_{139}$. A drastic change of the relative intensities of the diffraction peaks can be clearly observed after loading Ag into the ZX-V structure. This is mainly related to the change of the cationic composition between the two Faujasites. The deduced chemical formula of the Ag@ZX-V is $\text{Ag}_{27}\text{Na}_{55}\text{Al}_{73}\text{Si}_{119}\text{O}_{384}(\text{H}_2\text{O})_{120}$ with the stoichiometric sum of the $\text{Ag}_n^{\delta+}$ and Na^+ cations equal to 82, as previously observed for ZX-V. It should be noted that no diffraction peaks of metal oxide ($\text{M} = \text{V}, \text{Ag}$) phases were detected in the XRD patterns. This results show that the V content (0.25 wt.% V) is below the detection limit of XRD. The absence of silver peaks is due to the small size of highly dispersed silver phase in the fresh sample.

Figure 1(B) shows that both ZX-V and Ag@ZX-V samples exhibit a combination of Type I and IV isotherms with a H3-type hysteresis. The surface areas and pore volumes of ZX-V and Ag@ZX-V samples are summarized in Table 2.

Table 1.

The Ag@ZX-V catalyst exhibits a significantly decreased specific surface area (369 m²/g) and micropore volume (0.091 cm³/g) as compared with the parent ZX-V catalyst ($S_{BET} = 689$ m²/g; $V_{mic} = 0.185$ cm³/g). The mesoporosity was also decreased from 1.098 to 0.839 cm³/g after Ag loading into ZX-V structure. This decrease can be attributed to the partial pores blockage by Ag species and the higher density of silver particles.

The high resolution HAADF-STEM images of Ag@ZX-V sample are presented in Fig. 2. The Ag sub-nanoparticles appear as bright white dots within the pores of FAU-type structure. Ag-free ZX-V crystallites can also be observed in Figure 2(a) with a crystal size lower than 10 nm. The distribution of silver clusters in the zeolite is not perfectly uniform (some pores are empty or not completely filled; Fig. 2c) which in agreement with the loss of external surface area of ZX-V after Ag loading (Table 2). It should be noted that segregation of Ag nanoparticles from the pores into larger Ag nanoparticles can be obtained after the second scan by e-beam inside the microscope during imaging (Fig. S2). The EDS mapping of the Ag@ZX-V is reported in Fig. S3. The result confirms the good dispersion of the silver in the zeolite. However, this result should be interpreted with precaution due to the low stability of the silver particles under the electron beam (Fig. S2). More details concerning this phenomenon are reported in our previous paper (El-Roz et al., 2018).

Figure 2.

The DR-UV-Vis spectra of ZX-V and Ag@ZX-V and activated Ag@ZX-V at 150°C under Ar are illustrated in Fig. 3. For ZX-V, only one broad band was observed in the region of 250-285 nm, with a maximum at 270 nm. This is attributed to the low-energy charge transfer band (LCT) associated with O to V⁴⁺ electron transfer. This result points out that the amount of polymeric V⁵⁺ oxides is negligible and that namely isolated interstitial V⁴⁺ species are present. The ICP and EDX analyses of the ZX-V sample showed that vanadium content is around 0.25

wt. %. The characterization and localization of vanadate species was difficult due to their relatively low amount in the zeolite. It is clear, however, that oxalate-vanadate species are highly dispersed within the zeolite structure as clusters and no large aggregates are formed.

Figure 3.

The DR-UV-Vis spectrum of Ag@ZX-V powder shows the appearance of new UV-visible bands at 270, 295, 325, 377, 414nm. The bands between 270 and 380 nm are characteristic of the electronic transitions of reduced Ag species ($\text{Ag}_n^{\delta+}$) with sub-nanometer particles size (Gurin *et al.*, 2002; Severance *et al.* 2014). In addition, new bands at 432 and 562 nm attributed to the formation of silver nano-particles with a particle size >12 nm and >20 nm are also observed (Cuong *et al.*, 2013; Zou *et al.*, 2007). The presence of narrow UV bands at specific wavelength indicates that the silver clusters have well-defined size and charge. The visible bands (400-530 nm) can be attributed to the external silver nanoparticles as well as to the connected silver clusters within the network of the zeolite pores.

It should be noted that the same bands are observed in the Ag@ZX-V suspension (Fig. S4). This demonstrates the good stability of the prepared clusters in their solid forms under aerated condition. The shift observed in some absorption band can occur due to a solvatochrom effect. After in-situ activation of the sample at 150°C (under Ar), an increase of the broad plasmonic band has been observed in the visible range. This is most probably due to the migration of the silver clusters and their aggregation promoting the formation of silver nanoparticles. This phenomenon was already observed under the TEM beam (Fig. S2).

The infrared spectroscopy of adsorbed CO was used to determine the oxidation state of silver nanoparticles (Fig. 4). It is well known that surface carbonyls with zero-valent silver atoms cannot be formed at room temperature (Hadjivanov *et al.*, 2002). No characteristic bands

of carbonyl groups are observed in the ZX-V spectra, while an intense band at 2185 cm^{-1} is obtained after CO adsorption on Ag@ZX-V (Fig. 4(A)). This band is attributed to Ag^+ ions, mainly located inside the pores (Hadjivanov *et al.*, 2002). It is formed by multiple components (Fig. 4(B)) likely due to different silver clusters inside the zeolite. As the equilibrium pressure increases (Fig. 4(B)), another component appears at $\sim 2135\text{ cm}^{-1}$, which is characteristic of physisorbed CO on $\text{Ag}_n^{\delta+}$.

Figure 4.

2.2. Catalytic activity in the photo-assisted SCR- NH_3 reaction

The physicochemical properties, such as specific surface area, Si/Al ratio, acidity, stability and redox ability of metal-exchanged zeolite catalysts are strongly correlated to the catalytic performances for NO_x removal during the SCR process. It is generally recognized that both adsorbed ammonia on Lewis acid sites and ammonium ions associated with Brønsted acid sites are precursors to an activated site that can selectively reduce NO_x via different possible mechanisms of low-temperature NH_3 -SCR reaction, combining redox and acid-base steps (Gao *et al.* 2017; Iwasaki *et al.*, 2014; I. Nova *et al.*; 2014). These concepts can be summarized and described through an Eley-Rideal (ER) mechanism, where the gaseous NO first reacts with activated NH_3 -adsorbed species to form intermediates and then decomposes into N_2 and H_2O , or via a Langmuir-Hinshelwood (LH) mechanism, where the gaseous NO is adsorbed on a basic site and further combine with the adjacent activated NH_3 species to form N_2 and H_2O . According to previous reports regarding the SCR process over metal-exchanged zeolites (Devadas *et al.*, 2006; Long *et al.*, 2002), the presence of Brønsted acid sites is essential for achieving a high NO_x conversion and high N_2 selectivity. The Brønsted acid sites are involved

in the reaction by chemically binding and activating the ammonia to form ammonium ions, which then participates in the SCR reaction.

On the other hand, Bin *et al.* (2012) show that the existence of Brønsted acid sites contributes to an excellent dispersion of metal species within the zeolite structure. More recent studies have lowered the importance of these sites in the SCR mechanism (Janssens *et al.*, 2015). In our study, the FAU-X based samples do not possess any Brønsted acid site due to its sodium form with a low Si to Al molar ratio ($\text{Si/Al} = 1.63$). This is confirmed by the IR spectra of the ZX, ZX-V and Ag@ZX-V samples (Fig. S5), showing only one band at 3738 cm^{-1} in the O-H region characteristic of terminal Si-OH group (Deka *et al.*, 1998). However, the formation of acid sites during the reaction on Ag@ZX-V cannot be excluded due to the presence of NH_3 and H_2O in the gas phase. Thus, the monitoring of ZX-V and Ag@ZX-V samples in the photo-assisted SCR- NH_3 reaction at RT and at relatively low temperature ($T = 150 \text{ }^\circ\text{C}$) is of utmost importance. Then, some possible structure-activity relationships can be discussed by comparing the data obtained during the catalytic test with those relevant to their physico-chemical properties.

NO_x conversions during the photo-SCR

Figure 5 shows the conversion of NO, NO₂, and total NO_x during the photo-SCR at RT over the ZX-V and Ag@ZX-V catalysts. The values are determined by chemiluminescence at the steady state after 4 hours of visible-light irradiation. The NO_x values were subtracted from those obtained at the steady state in dark at RT. Each experiment was repeated at least two to three times, with an estimated uncertainty of about $\pm 5\%$. It should be noted that it was difficult to estimate the ammonia conversions during the photo-SCR, due to the low intensity of the NH_3 IR band in the gas phase.

Figure 5.

Figure 5 illustrates the activity of both catalysts at RT temperature under visible light. There is no significant activity (in the error range) observed over ZX-V, while negative conversions were obtained over Ag@ZX-V catalyst. The negative values obtained over Ag@ZX-V correspond to an increase of the NO, NO₂ and NO_x amount in the gas flow due to ammonia photooxidation. It should be noted that Ag⁺-ZX-V, prepared by a simple ionic exchange (no silver reduction), was also tested under similar previous conditions and no photocatalytic activity was observed (Fig. S6). This result indicates that the highly dispersed Ag^{nδ+} clusters in the zeolite matrix play a crucial role in the properties of a plasmonic photocatalyst. The significant amount of NO₂ (14.4 % of conversion) detected at the steady-state of the photocatalytic reaction at RT (Fig. 5), indicates possible oxidation of NO into NO₂ over Ag@ZX-V. The capacity of silver nanoparticles in the ammonia oxidation at relatively low temperature is already reported in the literature by using Ag/Al₂O₃ catalyst (Wang *et al.*, 2018). The authors show that both the valence state and particle size of Ag species had a significant influence on the catalyst activity for the ammonia oxidation to NO.

Increasing the temperature from RT to 150 °C does not influence the performance of ZX-V in both dark and under visible light irradiation conditions, and no significant activity is observed (Figure 6(A)). This result is due to the absence of active sites for SCR on ZX-V and the lack in the active species with absorption edges in the visible-light region. Same behavior of Ag@ZX-V can be observed at 150°C in dark without any significant catalytic activity. On the contrary, the activity of the Ag@ZX-V sample was radically changed under visible irradiation at 150°C (Fig. 6(B)). Loading of uniform, sub-nanosized and stable silver particles in the ZX-V material improves the NO_x conversion from 0.2 ±5 % (in dark) to more than 14.7

± 5 % (under visible light). It is to highlight that during the SCR experiments, no side products as N_2O were detected in the outlet, witnessing for 100 % selectivity to N_2 . The CO and HC conversions were also investigated during the photo-assisted SCR reaction at RT and $T = 150$ °C (supplementary data, Fig. S7). All conversions are negligible over both ZX-V and Ag@ZX-V samples under the different conditions used in this work.

Figure 6.

Evolution of surface species during the photo-SCR

The FTIR spectra of the catalysts at the steady-state of the SCR- NH_3 reaction are presented in Fig. 7.

Figure 7.

In the absence of irradiations at RT (spectra a, Fig. 7), a band centered at 1642 cm^{-1} , characteristic of NH_3 coordinated to Lewis acid sites (Rasmussen *et al.* 2018; Hamoud *et al.*, 2019), is observed for both samples. It can be strongly overlapped with the vibration band of adsorbed water. It is important to note that this band is more intense (saturated) and pronounced in case of ZX-V than for Ag@ZX-V. In addition, traces of band of ammonium cations can be observed, associated with the weak band at 1442 cm^{-1} (spectra a, Fig. 7), due to the presence of silica impurities that provide weak Brønsted acid sites (Gallardo *et al.*, 1997). Such silica phase (quartz) was detected in the X-ray diffraction patterns of ZX-V and Ag@ZX-V (see part 2.1.). No significant changes were observed in the IR spectra of ZX-V under visible irradiation at RT

(spectrum b, Fig. 7(A)). This is in agreement with the absence of any photocatalytic activity of this sample at RT.

In contrast, the intensity of the band at 1642 cm^{-1} of Ag@ZX-V is significantly decreased when the visible light is switched on (spectrum b, Fig. 7(B)). This is probably related to water desorption and/or NH_3 desorption/conversion. Under visible irradiation, a new broad band appeared at 1400 cm^{-1} belonging to the asymmetric vibration of adsorbed NH_3 on the Brønsted acid sites (formation of NH_4^+) (Strömet *al.* 2018). This is confirmed by the less pronounced absorption bands at 3260 and 3300 cm^{-1} , assigned to the symmetric and asymmetric N–H stretching vibrations of NH_3 hydrogen bonded to surface OH (Fig. S8). Thus, the development of the band at 1400 cm^{-1} indicates the *in-situ* formation of new B.A.S. on the zeolite during the reaction, promoted by water dissociation and/or ammonia oxidation. The *in situ* formation of B.A.S. has been already reported in the literature (Rasmussen *et al.* 2018; Ström *et al.* 2018) and authors showed that water can hydrolyze metal sites (Al, $\text{Ag}_n^{\delta+}$ clusters and/or vanadia species) of the catalyst creating new Brønsted acid sites. Also, the adsorbed ammonia is either directly consumed by the SCR reaction or converted into ammonium, which then participates in the SCR.

As the temperature increased from RT to $150\text{ }^\circ\text{C}$, the intensity of the band at 1642 cm^{-1} decreased rapidly, indicating the water/ammonia desorption. The other band located at 1400 cm^{-1} is appeared clearly in the spectra of ZX-V and is become more intense (saturated) in the case of Ag@ZX-V (spectrum (c), Fig.7). In fact, water molecules might strongly adsorb and fully occupy the adsorption sites of ZX-V at RT, preventing the adsorption of NH_3 on the B.A.S (Fig. S9). However, when the reaction temperature increases to $150\text{ }^\circ\text{C}$, more water molecules would desorb and release the active sites. As a result, the formation of NH_4^+ on the Brønsted acid sites of ZX-V is now clearly visible at $T = 150\text{ }^\circ\text{C}$. However, the negligible catalytic

activity of ZX-V and Ag@ZX-V at 150 °C (in dark) reveals that the formation of NH_4^+ is not enough for promoting the de NO_x process. Under visible light irradiation at 150 °C, no modification in the IR spectrum of ZX-V surface is observed, as expected. However, a significant decrease of the bands at 1642 cm^{-1} and 1400 cm^{-1} are observed on the Ag@ZX-V (spectrum (d), Fig. 7).

The *operando* FTIR results on Ag@ZX-V reveal more information on the evolution of the surface species as a function of time during the photo-SCR reaction. The results are reported in Fig. 8. The data help to envisage the interplay between the pre-adsorbed species, ammonia and ammonium ions. While the band of NH_3 bending vibrations at Lewis acid sites continuously decreases, a significant increase of the band at 1400 cm^{-1} , assigned to the vibrations of the ammonium ions at Brønsted acid sites, is observed during the reaction at RT under visible light (Fig. 8(A)). The irradiation of the Ag@ZX-V with visible light at 150°C under reaction flow (Fig. 8(B)) led to a quick decrease of water, ammonium and ammonia bands.

Figure 8.

Fig. 9 illustrates the evolution of NO_x concentrations versus the reaction time at RT and 150 °C in dark and during the irradiation. At RT (Fig. 9(A)), the concentration of the NO_x is gradually increased in the first few minutes of irradiation before reaching the plateau due to the possible oxidation of NH_3 into NO and/or NO_2 . In contrast, the concentration of NO_x drops rapidly when the lamp is turned on at 150 °C (Fig. 9(B)), indicating that the photo-assisted SCR reaction is taking place, via a possible photo-decomposition of an $\text{NH}_3\text{-NO}_x$ intermediate.

Figure 9.

The time-evolution of NH_4^+ (1400 cm^{-1}) and NH_3 overlapped by water adsorption (1642 cm^{-1}) band areas over Ag@ZX-V during SCR- NH_3 reaction at RT and $150\text{ }^\circ\text{C}$ is shown on Fig. 10. The main observation from this experiment is the significant and sudden drop of all species (and especially ammonia) when the visible light is turned on, at all temperatures, except for NH_4^+ at RT (Fig. 10(A)). In contrast, no changes in ammonia evolution were observed over ZX-V under similar conditions (supplementary data, Fig. S10). Otherwise, the NH_4^+ ions are continuously formed on ZX-V during the reaction at $150\text{ }^\circ\text{C}$, confirming that the only conversion of ammonia into ammonium cannot promote the SCR at $150\text{ }^\circ\text{C}$. These results with the catalytic activity confirm the photo-assisted SCR reaction over Ag@ZX-V with high selectivity.

Figure 10.

2.3. Mechanism

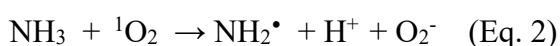
In summary, the set of the previous experimental data revealed that the ZX-V sample was completely inactive during the photo-assisted SCR-reaction at RT and at $T = 150\text{ }^\circ\text{C}$. In contrast, the reaction under visible irradiation seems to favor the oxidizing pathway to generate NO and NO_2 at RT over Ag@ZX-V , while the photo-assisted NO_x reduction is promoted at $T = 150\text{ }^\circ\text{C}$. In this part, the physico-chemical properties of Ag@ZX-V , as well as the reaction mechanism proposed in the literature, can be used to get insights in the photo-assisted SCR pathway over Ag@ZX-V at $T = 150\text{ }^\circ\text{C}$.

Progressive hydroxylation for supported zeolite with pure Lewis acidity indicates that a significant amount of water molecules will adsorb dissociatively, hydroxylating the zeolite

support and hydrolyzing the M-O bonds (M = Al or Ag), thus leading to the co-existence of Lewis and Brønsted acid sites. The formation of new Brønsted acid sites by hydroxylation induces the transformation of adsorbed NH₃ into ammonium species. Temperature and presence/absence of visible light conditions modulate the Lewis/Brønsted ratio up to the eventual total solvation of the zeolite by molecular adsorption of water. At RT and in the dark, the water molecules might strongly adsorb and fully occupy the adsorption sites of the catalyst. This can hinder the access of NH₃ molecule to the zeolite and partially inhibits the formation of NH₄⁺ on the Brønsted acid sites. Under visible irradiation and/or by increasing the temperature, the formation of ammonium species is promoted by partial desorption of water. On the other hand, NH₃ can also be linked to the free Ag Lewis sites. The presence of both adsorbed NH₃ and NH₄⁺ is indispensable for the photo-SCR reaction.

In a classical semiconductor photocatalyst (Shishido *et al.*, 2011; Li *et al.*, 2018), the UV or visible excitation can promote the formation of electron and holes by the excitation of an electron occupying the valence band, transferring it into the conduction band. The produced holes promote the oxidation, and the conduction band electrons promote the reduction of the adsorbed species. However, in the case of metallic clusters, the localized surface plasmon resonance (LSPR) is the unique optical phenomenon that occurs. When the frequency of incident light matches the oscillation frequency of the electrons of the conduction band of the metal, it triggers a collective excitation of the electrons. These excited surface electrons (hot electrons) oscillate coherently with the incident electromagnetic field. Then, hot electrons relax through a multi-step process initially involving electron–electron scattering, and then on a much slower timescale, transferring energy from the thermalized electron gas to the metal lattice via electron–phonon coupling, causing an interaction between the metal lattice and its surroundings (phonon–phonon interactions) (Liu & Li; 2016). This non-radiative LSPR relaxation process converts the kinetic energy of hot electrons into thermal energy heating up

quickly the surroundings of a metal surface. The generated heat can promote redox reactions that require a high temperature in dark conditions. One of the possible explanations of the photocatalytic activity of Ag@ZX-V at RT is the formation of oxidant species able to oxidize ammonium into NO, and NO into NO₂. Recently, Planas *et al.* (2016) demonstrated that silver nanoparticles could enhance the formation of singlet oxygen (¹O₂). More recently, Macia *et al.* (2018) demonstrated an impressive plasmon-enhanced singlet oxygen production on hybrid silver nanocubes. However, in the previously cited works, the formation of singlet oxygen through direct sensitization by metal nanoparticles was not investigated, and the role of the plasmon was limited to the enhancement of the singlet oxygen production via a grafted photosensitizer (Rose Bengal). The unprecedented and well demonstrated observation of singlet oxygen formation through direct sensitization by metal nanoparticles (Ag, Au, Pt) is, however, demonstrated by Vankayala *et al.* (2011). The singlet oxygen is well known for his capacity to generate highly oxidant OH and/or peroxide in the presence of labile hydrogen (in our case, the hydrogen of the ammonium) (Insug *et al.*, 2015; Rinalducci *et al.*, 2004). Therefore, the active site for the photo-oxidation at RT should be the Lewis acid site on Ag clusters, and the adsorption of NH₃ onto the Lewis acid site would be the first step in the photo-oxidation. The adsorbed NH₃ on Ag clusters (Lewis acid sites) could be activated by singlet oxygen to the NH₂ radical under visible light (Eq. 2). The NH₂ radical further reacts with the singlet oxygen to form NO (Eq. 3). The singlet oxygen can also oxidize NO into NO₂ (Eq. 4).



When the temperature increases from 25 to 150 °C under visible irradiation, the route of NH₃ reduction is more favorable than the ammonia oxidation pathway. The NH₃ reduction is promoted by the local plasmonic heating under visible light, which induces the thermal

decomposition of $\text{NH}_3\text{-NO}_x$ intermediates. In fact, the irradiation by visible light at 150°C leads to significant heating of the catalyst and thus the apparent temperature at the contact point would be higher than 150°C . Consequently, the SCR can operate at the low-temperature range in the presence of visible irradiation without increasing the temperature. This is confirmed by comparing the SCR activity of Ag@ZX-V at 150°C under visible light and at 200°C in dark (Fig. S11). The catalyst shows a good SCR activity under both conditions, with however higher NO_x conversions at 200°C . When the lamp is turned on at 150°C (Fig. 11(B)), the concentration of surface ammonium species is progressively consumed while the chemisorbed ammonia on Lewis sites has completely disappeared. Our results show that the NH_3 adsorbed on Lewis acid sites is preferentially consumed during the photo-SCR reaction, then the NH_4^+ species linked to the Brønsted acid site (which react slowly) migrate to the Lewis acid sites and participates in the reaction. The Brønsted sites act primarily as NH_3 storage sites during the photo-assisted SCR reaction. The adsorbed NH_3 on Lewis acid site is most likely activated to the NH_2 radical under visible irradiation. The NO_x species could react with NH_2 radical formed under visible irradiation, and N_2 would be selectively produced via nitrosoamide species (NH_2NO_2 and NH_2NO) (Eq. 5). Shishido *et al.* (2011) confirmed the formation of nitrosamide species (NH_2NO) by FTIR spectroscopy, with characteristic new bands between 1400 and 1600 cm^{-1} . Participation of nitrosamide species, as alternative intermediate, in the formation of N_2 and H_2O (Eq. 6) seems to be doubtful in our case, since no indication of such species was observed in our FTIR spectra. Alternatively, we can assume that they were rapidly decomposed during the reaction. However, it is expected that surface NH_2NO species are the major intermediates participating in the formation of N_2 over the Ag-based catalyst (Kondratenko *et al.*, 2008; Strom *et al.*, 2018; Shimizu *et al.*, 2017; Kondratenko *et al.*, 2008).



Based on this information and our previous results, the mechanism of the oxidation of NH_3 and reduction of NO , at room temperature and $150\text{ }^\circ\text{C}$, respectively, can be proposed as follow: at room temperature, the excitation of the silver particle promotes the formation of singlet oxygen, this later oxidize NH_3 first into NH_2 and then to NO . The oxidation of NO by singlet oxygen forming NO_2 can also take place. H^+ can also be produced from this oxidation process to form the NH_4^+ species detected on the surface of the catalyst. At $150\text{ }^\circ\text{C}$, the produced NH_2 under visible light can interact with NO and/or NO_2 to form NH_2NO and NH_2NO_2 , respectively. The dissociation of these intermediates to N_2 and H_2O is promoted by the local heating and traduced by a photo-assisted SCR process. The mechanism of the reaction is illustrated in scheme 1.

Scheme 1.

2.4. Conclusions

In summary, sub-nanometer silver clusters in FAU-type zeolite containing vanadate clusters were synthesized and evaluated during the photo-assisted SCR- NH_3 reaction under visible light at RT and $150\text{ }^\circ\text{C}$. The Ag-free sample was completely inactive during the photo-assisted SCR-reaction under studied conditions.,In contrast, $\text{Ag}@Z\text{X-V}$ revealed a photocatalytic activity under visible light promoted by the high dispersion and the good accessibility of the generated silver nanoparticles. The *operando* FTIR technique revealed the *in-situ* formation of Bronsted acid sites on $\text{Ag}@Z\text{X-V}$ catalyst which play the role of storing and supplying the NH_3 species to the active sites. Further the ammonia activation by singlet oxygen to possibly yield NH_2 radicals is most probably a result of the direct sensitization by $\text{Ag}_n^{\delta+}$ clusters/nanoparticles under visible irradiation. At room temperature, the singlet oxygen can further oxidize NH_2 radical to NO as well as NO to NO_2 . However, the main reaction pathway leading to N_2 is the thermal decomposition of NH_2NO intermediates, formed from

NO and adsorbed NH₂ fragments. This SCR pathway is probably promoted by the local plasmonic heating of the catalyst at 150 °C and under visible light. However, further experiments are required to investigate the reaction intermediates that are not detected in the present study, likely due to their short lifetime.

Acknowledgment

Authors acknowledge the PHC-Tassili project (17MDU983) and the Normandy Region (RHIN, RAPHYD project) for supporting this work.

References

- Bin, F., Song, C., Lv, G., Song, J., Cao, X., Pang, H., & Wang, K. (2012). Structural characterization and selective catalytic reduction of nitrogen oxides with ammonia: a comparison between Co/ZSM-5 and Co/SBA-15. *J. Phys. Chem. C*, 116, 26262-26274.
- Castoldi, L., Bonzi, R., Lietti, L., Forzatti, P., Morandi, S., Ghiotti, G., & Dzwigaj, S. (2011). Catalytic behaviour of hybrid LNT/SCR systems: Reactivity and in situ FTIR study. *J. Catal.* 282, 128-144.
- Chen, M., Yang, J., Liu, Y., Li, W., Fan, J., Ran and Dou, S. X. (2015). TiO₂ interpenetrating networks decorated with SnO₂ nanocrystals: enhanced activity of selective catalytic reduction of NO with NH₃. *J. Mater. Chem.* 3, 1405-1409.
- Cuong, N. T., Nguyen, H. M. T., & Nguyen, M. T. (2013). Theoretical modeling of optical properties of Ag 8 and Ag 14 silver clusters embedded in an LTA sodalite zeolite cavity. *Phys. Chem. Chem. Phys.*, 15, 15404-15415.
- Deka, R. C. (1998). Acidity in zeolites and their characterization by different spectroscopic methods.
- Devadas, M., Kröcher, O., Elsener, M., Wokaun, A., Söger, N., Pfeifer, M. & Musmann, L. (2006). Influence of NO₂ on the selective catalytic reduction of NO with ammonia over Fe-ZSM5. *Appl. Catal. B-Environ.* 67, 187-196.
- El-Roz, M., Telegeiev, I., Mordvinova, N. E., Lebedev, O. I., Barrier, N., Behilil, A. & Valtchev, V. (2018). Uniform Generation of Sub-nanometer Silver Clusters in Zeolite Cages Exhibiting High Photocatalytic Activity under Visible Light. *ACS Appl Mater Interfaces.* 10, 28702-28708.
- Gao, R., Zhang, D., Maitarad, P., Shi, L., Rungrotmongkol, T., Li and Cao, W. (2013). Morphology-dependent properties of MnO_x/ZrO₂-CeO₂ nanostructures for the selective catalytic reduction of NO with NH₃. *J. Phys. Chem. C*, 117, 10502-10511.
- Gao, F., Tang, X., Yi, H., Zhao, S., Li, C., Li, J., ... & Meng, X. (2017). A review on selective catalytic reduction of NO_x by NH₃ over Mn-based catalysts at low temperatures: catalysts, mechanisms, kinetics and DFT calculations. *Catal.*, 7, 199.
- Gallardo Amores, J. M., Sanchez Escribano, V., Ramis, G., & Busca, G. (1997). An FT-IR study of ammonia adsorption and oxidation over anatase-supported metal oxides. *Appl. Catal., B*, 13(1), 45-58.

- Gurin, V. S., Petranovskii, V. P., & Bogdanchikova, N. E. (2002). Metal clusters and nanoparticles assembled in zeolites: an example of stable materials with controllable particle size. *Mater Sci Eng C*, 19, 327-331.
- Hadjiivanov, K. I., & Vayssilov, G. N. (2002). Characterization of oxide surfaces and zeolites by carbon monoxide as an IR probe molecule.
- Hamoud, H. I., Valtchev, V., & Daturi, M. (2019). Selective Catalytic Reduction of NO_x over Cu- and Fe-exchanged zeolites and their mechanical mixture. *Appl. Catal. B-Environ.* doi.org/10.1016/j.apcatb.2019.02.022.
- Huang, Z., Li, H., Gao, J., Gu, X., Zheng, L., Hu & Chen, J. (2015). Alkali- and sulfur-resistant tungsten-based catalysts for NO_x emissions control. *Environ. Sci. Technol.* 49, 14460-14465.
- Iwasaki, M. (2014). Mechanistic Aspect of NO–NH₃–O₂ Reacting System. In *Urea-SCR Technology for deNO_x After Treatment of Diesel Exhausts* (pp. 221-246). Springer, New York, NY.
- Janssens, T. V., Falsig, H., Lundegaard, L. F., Vennestrøm, P. N., Rasmussen, S. B., Moses, P. G & Bordiga, S. (2015). A consistent reaction scheme for the selective catalytic reduction of nitrogen oxides with ammonia. *ACS Catal.* 5, 2832-2845.
- Kolobova, E., Pestryakov, A., Shemeryankina, A., Kotolevich, Y., Martynyuk, O., Vazquez, H. T., & Bogdanchikova, N. (2014). Formation of silver active states in Ag/ZSM-5 catalysts for CO oxidation. *Fuel*, 138, 65-71.
- Kondratenko, V. A., Bentrup, U., Richter, M., Hansen, T. W., & Kondratenko, E. V. (2008). Mechanistic aspects of N₂O and N₂ formation in NO reduction by NH₃ over Ag/Al₂O₃: The effect of O₂ and H₂. *Appl. Catal. B-Environ* 84, 497-504.
- Larrubia, M. A., Ramis, G., & Busca, G. (2001). An FT-IR study of the adsorption and oxidation of N-containing compounds over Fe₂O₃-TiO₂ SCR catalysts. *Appl. Catal. B-Environ.* 30(1-2), 101-110.
- Li, X., Yan, X., Lu, X., Zuo, S., Li, Z., Yao, C., & Ni, C. (2018). Photo-assisted selective catalytic reduction of NO by Z-scheme natural clay based photocatalyst: Insight into the effect of graphene coupling. *J. of catal.* 357, 59-68.
- Liu, T., & Li, Y. (2016). Photocatalysis: Plasmonic solar desalination. *Nat. Photon.*, 10, 361.
- Long, R. Q., & Yang, R. T. (2002). Reaction mechanism of selective catalytic reduction of NO with NH₃ over Fe-ZSM-5 catalyst. *J. catal.*, 207, 224-231.
- Macia, N., Bresoli-Obach, R., Nonell, S., & Heyne, B. (2018). Hybrid Silver Nanocubes for Improved Plasmon-Enhanced Singlet Oxygen Production and Inactivation of Bacteria. *JACS*. 141, 684-692.
- Malpartida, I., Marie, O., Bazin, P., Daturi, M., & Jeandel, X. (2011). An operando IR study of the unburnt HC effect on the activity of a commercial automotive catalyst for NH₃-SCR. *Appl. Catal., B. Environ.* 102, 190-200.
- Nova, I., & Tronconi, E. (Eds.). (2014). *Urea-SCR technology for deNO_x after treatment of diesel exhausts* (pp. 6-25). New York: Springer.
- Palatinus, L., & Chapuis, G. (2007). SUPERFLIP—a computer program for the solution of crystal structures by charge flipping in arbitrary dimensions. *J. Appl. Crystallogr.* 40, 786-790.
- Park, E., Kim, M., Jung, H., Chin, S., & Jung, J. (2013). Effect of sulfur on Mn/Ti catalysts prepared using chemical vapor condensation (CVC) for low-temperature NO reduction. *ACS Catal.* 3, 1518-1525.
- Planas, O., Macia, N., Agut, M., Nonell, S., & Heyne, B. (2016). Distance-dependent plasmon-enhanced singlet oxygen production and emission for bacterial inactivation. *JACS*. 138, 2762-2768.

- Rasmussen, S. B., Portela, R., Bazin, P., Ávila, P., Bañares, M. A., & Daturi, M. (2018). Transient operando study on the $\text{NH}_3/\text{NH}_4^+$ interplay in V-SCR monolithic catalysts. *Appl. Catal. B-Environ* 224, 109-115.
- Rinalducci, S., Pedersen, J. Z., & Zolla, L. (2004). Formation of radicals from singlet oxygen produced during photoinhibition of isolated light-harvesting proteins of photosystem II. *BiochimBiophys Acta Bioenerg.* 1608, 63-73.
- Severance, M., & Dutta, P. K. (2014). Evolution of silver nanoparticles within an aqueous dispersion of nanosized Zeolite Y: mechanism and applications. *J. Phys. Chem. C.* 118, 28580-28591.
- Shimizu, K. I., & Satsuma, A. (2007). Reaction mechanism of H_2 -promoted selective catalytic reduction of NO with NH_3 over $\text{Ag}/\text{Al}_2\text{O}_3$. *J. Phys. Chem. C.* 111, 2259-2264.
- Shishido, T., Teramura, K., & Tanaka, T. (2011). A unique photo-activation mechanism by “in situ doping” for photo-assisted selective NO reduction with ammonia over TiO_2 and photooxidation of alcohols over Nb_2O_5 . *Catal. Sci. & Technol.*, 1, 541-551.
- Ström, L., Carlsson, P. A., Skoglundh, M., & Hårelind, H. (2018). Surface species and metal oxidation state during H_2 -assisted NH_3 -SCR of NO_x over alumina-supported silver and indium. *Catal.* 8, 38.
- Thirupathi, B. and Smirniotis, P. G. (2011). Co-doping a metal (Cr, Fe, Co, Ni, Cu, Zn, Ce, and Zr) on Mn/TiO_2 catalyst and its effect on the selective reduction of NO with NH_3 at low-temperatures. *Appl. Catal. B-Environ.* 110, 195-206.
- Vankayala, R., Sagadevan, A., Vijayaraghavan, P., Kuo, C. L., & Hwang, K. C. (2011). Metal nanoparticles sensitize the formation of singlet oxygen. *Angew. Chem. Int. Ed.* 50, 10640-10644.
- Wang, F., Ma, J., He, G., Chen, M., Zhang, C., & He, H. (2018). Nanosize effect of Al_2O_3 in $\text{Ag}/\text{Al}_2\text{O}_3$ catalyst for the selective catalytic oxidation of ammonia. *ACS Catal.* 8, 2670-2682.
- Xu, L., & McCabe, R. W. (2012). LNT+ in situ SCR catalyst system for diesel emissions control. *Catal. Today*, 184, 83-94.
- Yamamoto, A., Teramura, K., Hosokawa, S., & Tanaka, T. (2015). Effects of SO_2 on selective catalytic reduction of NO with NH_3 over a TiO_2 photocatalyst. *Sci. Technol. Adv. Mater.* 16, 024901.
- Yamamoto, A., Teramura, K., Hosokawa, S., Shishido, T., & Tanaka, T. (2015). Visible-Light-Assisted Selective Catalytic Reduction of Nitric Oxide with Ammonia over Dye-Modified Titania Photocatalysts. *ChemCatChem*, 7, 1818-1825.
- Yamamoto, A., Mizuno, Y., Teramura, K., Hosokawa, S., Shishido, T., & Tanaka, T. (2015). Visible-light-assisted selective catalytic reduction of NO with NH_3 on porphyrin derivative-modified TiO_2 photocatalysts. *J. adv. catal. sci. technol.* 5, 556-561.
- Yamazoe, S., Masutani, Y., Teramura, K., Hitomi, Y., Shishido, T., & Tanaka, T. (2008). Promotion effect of tungsten oxide on photo-assisted selective catalytic reduction of NO with NH_3 over TiO_2 . *Appl. Catal. B Environ.* 83, 123-130.
- Yang, P., Zhang, J., Liu, D., Liu, M., Zhang, H., Zhao, P., & Zhang, C. (2018). Facile synthesis of porous nitrogen-doped carbon for aerobic oxidation of amines to imines. *Micropor. Mesopor. Mat.* 266, 198-203.
- Yen, H., Seo, Y., Kaliaguine, S., & Kleitz, F. (2012). Tailored mesostructured copper/ceria catalysts with enhanced performance for preferential oxidation of CO at low temperature. *Angew. Chem.* 124, 12198-12201.
- Zou, J., Xu, Y., Hou, B., Wu, D., & Sun, Y. (2007). Controlled growth of silver nanoparticles in a hydrothermal process. *China Particuology*, 5, 206-212.